Journal of Japan Association for Earthquake Engineering, Vol.15, No.3, 2015

VIBRATION CHARACTERISTICS OF HIGH-RISE STEEL BUILDING IN SHINJUKU SKYSCRAPER DISTRICT BEFORE AND AFTER THE 2011 OFF THE PACIFIC COAST OF TOHOKU EARTHQUAKE

Tetsuo YAMASHITA[1], Yoshiaki HISADA[2], Tomonari SAKAMOTO[3] and Tomohiro KUBO[4]

[1] Associate Professor, School of Architecture, Kogakuin University, Tokyo, Japan, tetsuo_y@cc.kogakuin.ac.jp
[2] Member of JAEE, Professor, School of Architecture, Kogakuin University, Tokyo, Japan, hisada@cc.kogakuin.ac.jp
[3] Graduate Student, Kogakuin University
[4] Assistant Professor, School of architecture of Kogakuin University

ABSTRACT: This paper presents and analyzes the identified vibration characteristics of steel high-rise building built at Shinjuku. The vibration characteristics, i.e.; natural periods, damping coefficients and participation functions, are identified from the measured acceleration during some earthquakes including the mainshock of the 2011 off the Pacific coast of Tohoku Earthquake. The curve-fitting method using the transfer function is applied in the identification. The change in natural period before and after the earthquake and the dependency on the modal amplitude are clear. The damping coefficients for the 1st and 2nd modes are found to be unexpectedly smaller than 0.02, that has been conventionally assumed in design of steel buildings.

Key Words: The 2011 off the Pacific coast of Tohoku Earthquake, Steel high-rise building, Vibration characteristics, Natural period, Damping coefficient, Participation function, Transfer function

1. INTRODUCTION

This report analyzes the record of observed acceleration of the steel high-rise building in Shinjuku Ward, Tokyo, constructed in an area where super high-rise buildings are concentrated in 1989, in the event of the 2011 off the Pacific coast of Tohoku Earthquake, and shows the vibration characteristics of natural periods, damping coefficients and other data in the area of large amplitudes of strong motions which could not be obtained before.

When the off the Pacific coast of Tohoku Earthquake occurred on March 11, 2011, intensity 5 lower was recorded in the area of super high-rise buildings in Shinjuku, Tokyo, which is approximately 400km away from the epicenter, and large tremors and damage were also observed in the super high-rise

buildings[1]. The response acceleration was recorded at the maximum of 300gal in the NS direction on the 29th floor at the Shinjuku Campus of Kogakuin University (29 floors above the ground and six underground floors) which this report conducted research on. There was damage, including the falling of ceilings and the breakdown of elevators[2].

The research conducted in the past about analysis of vibration characteristics on the basis of the observation record of a steel high-rise building includes the report by Kasai and others on identification of vibration characteristics of each building on the basis of the observation record of vibration-control, earthquake-resistant buildings in response to strong tremors of the Tohoku-Pacific Ocean Earthquake[3]. Yokota and others conducted research on regressive analysis of a relation between natural periods and damping coefficients in minute amplitude to relatively large amplitude from the measurement of slight motions, the vibration test, and the observation record of moderate earthquakes of about intensity 4 in connection with steel high-rise buildings with a period of two seconds and over[4]. Kashima and others identified vibration characteristics by analyzing the observation record of strong motions from 1990 to 2004 in 25 reinforced-concrete, steel-reinforced concrete, and steel buildings in the country, and showed a year-to-year change in amplitude dependency of natural periods and vibration characteristics[5]. Yamazaki and others calculated damping coefficients through the application of the RD method to the record from the microtremor measurement in about a dozen buildings of steel and concrete-filled steel tube structures in Aichi Prefecture, and indicated that most of the data were below the assumption made in the course of the design, and that high-mode damping was smaller than calculated data of damping proportional to rigidity[6]. Hirata and others confirmed the increase in natural periods in comparison with the continuous microtremor from the observation record of a 50-storied super high-rise building of concrete filled steel tube and steel-concrete structures in the event of the earthquake under the northwestern part of Chiba Prefecture in 2005, and compared the data with the analysis[7]. Yamada and others introduced examples of measurement of super high-rise seismic-isolated buildings[8].

The authors of this report and others identified natural periods and damping coefficients of the continuous microtremor and minute amplitude by human-powered vibration measurement of the building which this report is examining, and indicated that damping coefficients which corresponded to the primary and secondary modes were about 1%, respectively, and compared the observation record of earthquakes and response analysis of a 3D moment-frame structure[9]. However, the amplitude was slight, and the data for strong motions were unidentified. This report analyzes the record of response to strong motions in the event of the off the Pacific coast of Tohoku Earthquake, and identifies natural periods, damping coefficients and participation function up to the third mode in the event of a large amplitude. It also analyzes various scales of amplitudes before and after the main tremor, and the observation record of earthquakes of period characteristic in the same method, and observes a change in vibration characteristics.

2. OUTLINE OF STRUCTURE

2.1 Building frame and Cross section of materials

A three-dimensional CG figure of the building frame is indicated in Fig. 1a, a beam plan of the standard floor in Fig. 1b, and a framing elevation of the structure above the ground in Fig. 1c. The building which this report is examining is a super high-rise building of 29 floors above the ground (GL+127.8m) and six floors below the ground (GL-29.7m), constructed in 1989. With the steel construction above the ground and the steel-framed reinforced concrete construction below the ground, the building is supported by the reinforced concrete pressure-resistant slab of about 4.1m thickness on the Tokyo gravel layer. The structure of the underground part is integrated with a steel-frame super high-rise building of about the same height which is adjacent to the building under examination.

The two-dimensional figure of the standard floor is a rectangle of 38.4m in the EW direction and 25.5m in the NS direction, and is almost symmetrical except for some part of the lower floors, which does not cause torsional vibration. The characteristics of the frame are significantly shown in the EW direction. A double core of multi-story steel braces is located at each end, and large beams of 25.6m

span are bridged between them, on which classrooms are located. In addition, the whole areas on the 14th floor and 21st floor are super-truss structured for ensuring rigidity to horizontal power.

The building in the NS direction is a relatively simple rigid-frame structure with braces. Multi-story steel braces are located at intervals of one span at both core parts, and beams between them, functioning as a boundary beam, are subjected to relatively large shearing force and bending moment. Additionally, super-truss floors in the EW direction on the 14th and 21st floor are 5.5m high (3.9 to 4.3m on general floors), and are thus relatively low in terms of shearing rigidity.

The posts are BOX of welded-assembly with the use of SM490A (SM490B for lower parts). H-steel of welded assembly of SM490A, and SS400 in some parts are used for large beams and braces. Table 1a shows typical member sections of posts above the ground and braces and super-truss, and Table 1b shows cross sections of large beams. No energy dissipation device is utilized.

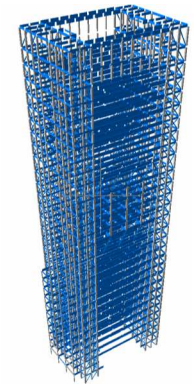

Fig. 1a Structure

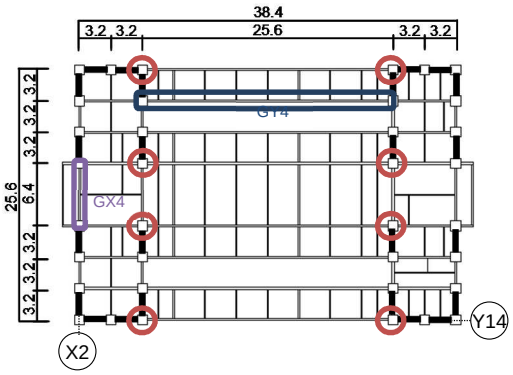

Fig. 1b Beam plan of the standard floor
(Thick line: location of braces, ○: C1 post)

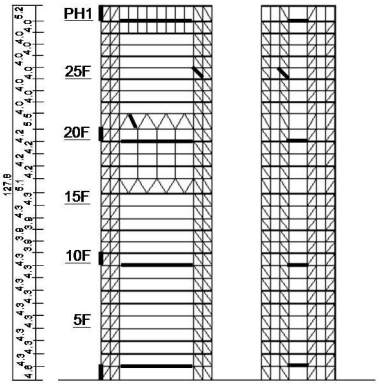

Fig. 1c Framing elevation

Table 1a Cross section of columns and braces

Floor	C1 Post	X2-street brace	Y14-street brace
PH1	□-488x19	BH-250x250x9x14	BH-250x250x9x14
20	□-508x28	BH-250x250x9x14	BH-250x250x12x16
10	□-544x47	BH-250x250x9x14	BH-250x250x19x19
1	□-600x75	BH-250x250x19x19	BH-250x250x19x25
14,21		(Super-truss)	BH-300x300x12x22

Table 1b Cross section of beams

Floor	Large beam(GX4)	Long-span beam(GY4)
PH1	BH-600x300x12x25	BH-1000x320x19x25
20	BH-600x350x12x32	BH-1000x300x19x28
10	BH-600x400x12x32	BH-1000x350x19x25
2	BH-600x350x12x32	BH-1000x320x19x25

2.2 Measurement of acceleration

The servo-type accelerometer conducts real-time measurement of earthquake response of the building under research[9]. Figure 2 indicates the location of measurement and its direction. The measurement on the floors is conducted for a depth of 100m, the 6th underground floor, the 1st, 8th, 16th, 22nd, 24th and 29th floors above ground with measurement of acceleration of two directions, NS (the short side) and EW (the long side). Two places are measured in the NS direction, and one place in the EW direction. Because this research is focused on vibration properties in the upper structure, the observation record of underground floors is not used. The observation record in the NS direction is analyzed with use of time history of acceleration which is obtained by an average of the observation record of two places. For the reference, the record on the 16th floor in the EW direction is hardly used due to the noise except for some part.

3. ACCELERATION RECORD OF EARTHQUAKE RESPONSE

3.1 Damage and record of measurement of principal earthquake of the off the Pacific coast of Tohoku Earthquake

Strong motions were observed even in the building under research in the event of the off the Pacific coast of Tohoku Earthquake on March 11, 2011. The maximum acceleration was recorded at 89gal and 92gal, respectively, on the first floor in the NS and EW directions, but on the 29th floor, it was 316gal and 235gal, respectively, which was amplified by approximately 3.6 times and 2.6 times, respectively (the data for the NS direction is an average of the record of the accelerograph at the two places).

Below is damage to the non-structural members caused by the tremor2). No one was hurt in this earthquake.

1) Falling of the ceiling panel (28th floor, Fig. 3a), and removal of the ceiling panel (24th floor)
2) Scattered books and others (25th floor, Fig. 3b)
3) Collapse of furniture and partition walls (24th floor)
4) Suspension of elevators: The building is equipped with the automatic stop system[15)] with the use of the emergency earthquake warning. In the event of the earthquake, it effectively functioned to stop all the seven elevators, but the freight elevator had trouble with its cable, and took about a month to be repaired.

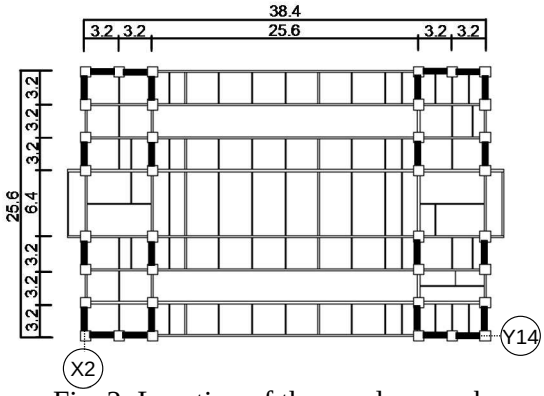

Fig. 2: Location of the accelerograph

Fig. 3a Falling of the ceiling panel (28th floor)

Fig. 3b Scattered books and others (25th floor)

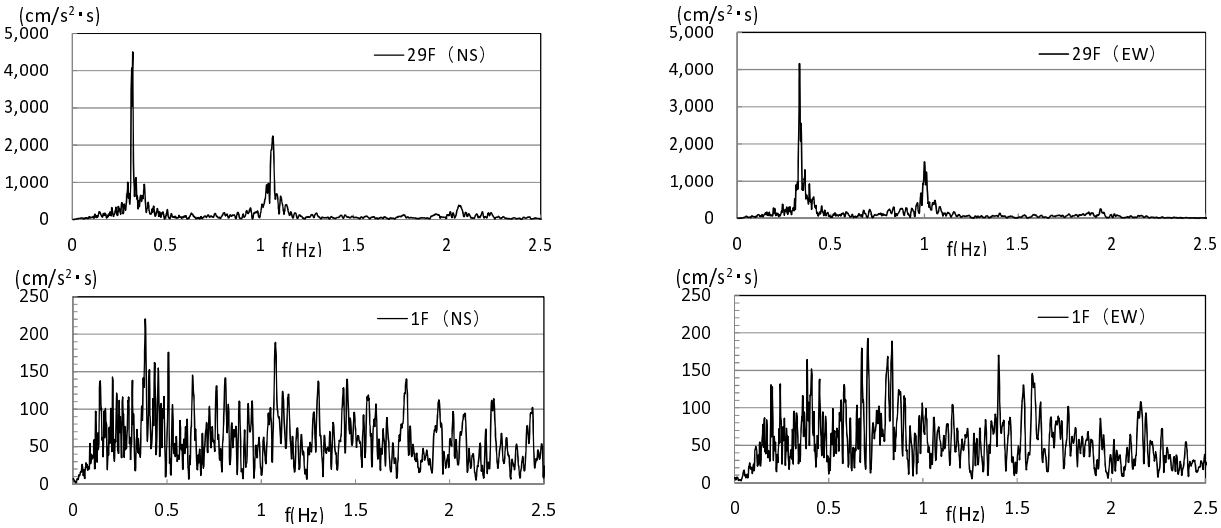

Fig. 4 Fourier spectrum of acceleration on the 1st and 29th floors

Appendix 1 (because of a large number of figures) indicates the time history of acceleration on aboveground floors in the event of the March 11 disaster. The disturbance of waveform in the EW direction on the 16th floor is assumed to have been caused by the mixture of noise. Fig. 4 shows Fourier spectrum on the 1st and 29th floors.

3.2 Measuring and record of other earthquakes

Table 3 shows a list of earthquake motions for identification of vibration characteristics. This paper uses the observation records of the Niigata Chuetsu Earthquake and the earthquake under the northwestern part of Chiba Prefecture prior to the March 11 earthquake. It uses the response record of four types of aftershocks and triggered earthquakes with different amplitude, including the largest aftershock of M7.7 with an epicenter off the Ibaraki coast which occurred approximately 30 minutes after the main earthquake. Fig. 5 shows the velocity response spectrum of the waveform of observed acceleration on the 1st floors (h=0.02).

4. ANALYSIS OF VIBRATION CHARACTERISTICS

4.1 Identification method of vibration characteristics

In this section, by the curve-fitting method using the transfer function[10], natural periods, damping coefficients and participation functions are identified. In detail, the ratio of the Fourier spectrum of the 1st floor to the one on the k floor in the record of acceleration is regarded as an observation record of a transfer function on the k floor. In calculation of a Fourier spectrum, the Hanning window is used once so as to smooth the Fourier spectrum.

For identification of vibration characteristics, a peak of the observation record of a transfer function is calculated first. Then, $|G_k(\omega)|$ (Eq. (1)) of real part of amplitude in theoretical solution of a transfer function for $e^{i\omega t}$ of harmonic motion of the period $T=2\pi/\omega$ which is gained from the mode development is conformed with the observation record with the use of the least-squares method, and h_j of a damping coefficient, β_j and $\phi_{j,k}$ of a participation function of the mode j are calculated. In such calculation, the natural period which is identified first is used as a definite value.

$$|G_k(\omega)| = \sqrt{G_{kR}(\omega)^2 + G_{kI}(\omega)^2}$$
$$G_{kR}(\omega) = \sum_{j=1}^{N} \frac{1+(2h_jB_j)^2 - B_j^{\,2}}{(1-B_j^{\,2})^2 + (2h_jB_j)^2} \cdot \beta_j\phi_{j,k}, \quad G_{kI}(\omega) = \sum_{j=1}^{N} \frac{-2h_jB_j^{\,3}}{(1-B_j^{\,2})^2 + (2h_jB_j)^2} \cdot \beta_j\phi_{j,k} \quad , \quad B_j = \frac{\omega}{\omega_j} \tag{1}$$

in which N is the maximum mode with a set of N=3, and the relevant range is 0.2-2.5Hz. Appendix 2 shows the relevance of transfer functions. Table 4a shows natural periods which are identified up to the third mode, and Table 4b shows the damping coefficients. Because there was very little difference by identified floor in natural periods, the mean value of each floor is indicated in Table 4s. Blank tables means unanalyzable cases due to the large effect of noise on the waveforms. In addition, Fig. 6 shows participation functions along with results of characteristic values of the three-dimensional model on the aboveground parts (see Appendix 3). The floors where participation functions were identified are also plotted.

Table 3 Earthquake motions to be used for identification

Indication	Name of earthquake	Date of occurrence	Time of occurrence	Scale	Epicentral distance (km)	Maximum acceleration (EW1F,cm/s^2)	Maximum acceleration (NS1F,cm/s^2)	Maximum acceleration (EW29F,cm/s^2)	Maximum acceleration (NS1F,cm/s^2)
Chuetsu	Niigata Prefecture Chuetsu Earthquake	2004/10/23	17:56	M6.8	194	8.9	8.7	21.9	26.2
Chiba	Earthquake under the northwestern part of Chiba Prefecture i	2008/5/8	7:34	M4.6	159	79.6	46.9	58.7	82.4
Main tremor	Off the Pacific coast of Tohoku Earthquake	2011/3/11	14:46	M9.0	388	91.9	88.5	234.6	316.2
Largest aftershock	Aftershock with an epicenter off the Ibaraki coast	2011/3/11	15:15	M7.7	169	32.8	33.7	80.1	118.8
Aftershock in Fukushima	Aftershock with an epicenter off the Fukushima coast	2011/3/11	16:17	M6.4	348	2.9	3.0	7.7	10.3
Aftershock in Ibaraki	Aftershock with an epicenter off the Ibaraki coast	2011/3/11	17:19	M6.8	164	5.0	4.4	18.7	10.1
Fukushima-hama	Earthquake under Hama-dori, Fukushima Prefecture	2011/4/11	17:16	M7.1	310	14.9	12.1	36.9	34.9

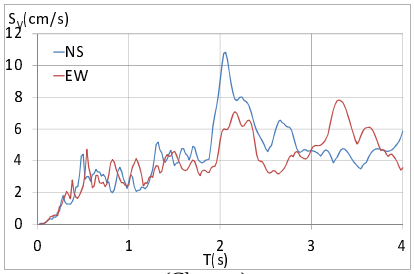

(Chuetsu)

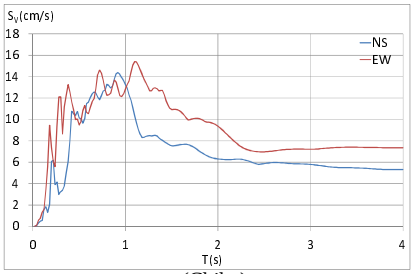

(Chiba)

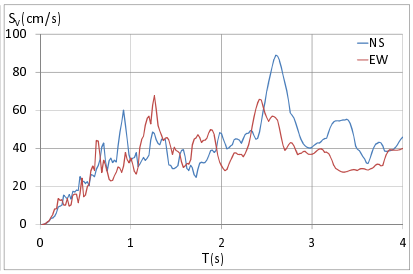

(Main tremor of the March 11 Earthquake)

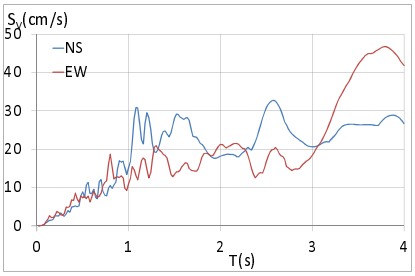

(Largest aftershock)

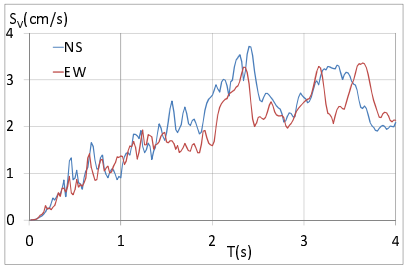

(Aftershock in Fukushima)

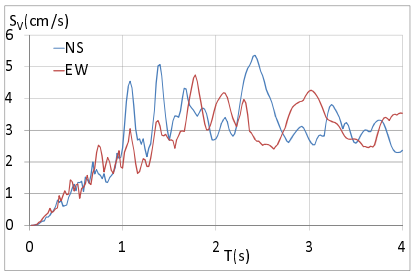

(Aftershock in Ibaraki)

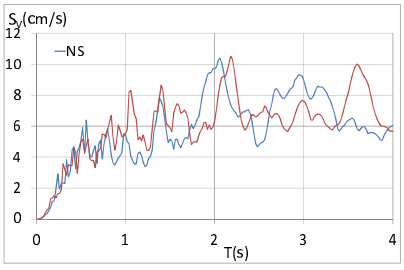

(Earthquake under the Hama-dori, Fukushima Prefecture)

Fig. 5 Velocity response spectrum of the input earthquake motions on the 1st floors (h=0.02)

Table 4a Natural periods (unit: s)

Direction	Mode	Chuetsu	Chiba	Main tremor	Largest aftershock	Aftershock in Fukushima	Aftershock in Ibaraki	Fukushima-hama	3D model (reference)
NS	1	2.91	2.91	3.08	3.12	3.06	3.01	3.06	3.09
	2	0.90	0.91	0.95	0.95	0.92	0.92	0.94	0.99
	3	0.45	0.46	0.47	0.48	0.47	0.46	0.48	0.51
EW	1	2.79	2.78	2.96	2.96	2.89	2.92	2.93	2.96
	2	0.92	0.96	0.99	1.00	0.96	0.96	0.98	1.03
	3	0.49	0.50	0.52	0.52	0.50	0.50	0.51	0.55

Table 4b Damping coefficients

(NS 1st)

Direction	Chuetsu	Chiba	Main tremor	Largest aftershock	Aftershock in Fukushima	Aftershock in Ibaraki	Fukushima-hama
29	0.011	0.008	0.018	0.011	0.017	0.013	0.012
22	0.011	0.008	0.019	0.011	0.016	0.013	0.012
16		0.008	0.019	0.011	0.015	0.013	0.013
8	0.011			0.013	0.015	0.013	0.012
Average	0.011	0.008	0.019	0.012	0.016	0.013	0.012
Overall average	0.013						

(EW 1st)

Direction	Chuetsu	Chiba	Main tremor	Largest aftershock	Aftershock in Fukushima	Aftershock in Ibaraki	Fukushima-hama
29	0.018	0.020	0.012	0.013	0.019	0.017	0.017
22	0.018	0.021	0.013	0.013	0.019	0.018	0.017
16					0.018		
8	0.018			0.012	0.019	0.017	0.017
Average	0.018	0.021	0.012	0.013	0.019	0.017	0.017
Overall average	0.017						

(NS 2nd)

Direction	Chuetsu	Chiba	Main tremor	Largest aftershock	Aftershock in Fukushima	Aftershock in Ibaraki	Fukushima-hama
29	0.017	0.011	0.012	0.012	0.015	0.017	0.008
22	0.016	0.009	0.012	0.009	0.014	0.018	0.008
16		0.012	0.012	0.012	0.015	0.016	0.007
8	0.016			0.013	0.015	0.015	0.007
Average	0.016	0.010	0.012	0.012	0.014	0.017	0.007
Overall average	0.013						

(EW 2nd)

Direction	Chuetsu	Chiba	Main tremor	Largest aftershock	Aftershock in Fukushima	Aftershock in Ibaraki	Fukushima-hama
29	0.018	0.030	0.032	0.027	0.019	0.025	0.024
22	0.022	0.024	0.027	0.022	0.020	0.024	0.024
16					0.027		
8	0.022			0.023	0.018	0.026	0.024
Average	0.021	0.027	0.029	0.024	0.021	0.025	0.024
Overall average	0.024						

(NS 3rd)

Direction	Chuetsu	Chiba	Main tremor	Largest aftershock	Aftershock in Fukushima	Aftershock in Ibaraki	Fukushima-hama
29	0.020	0.012	0.032	0.019	0.014	0.017	0.018
22	0.019	0.012	0.029	0.019	0.016	0.015	0.018
16		0.035	0.035	0.035	0.021	0.019	0.036
8	0.021			0.020	0.016	0.016	0.017
Average	0.020	0.020	0.032	0.023	0.017	0.017	0.022
Overall average	0.022						

(EW 3rd)

Direction	Chuetsu	Chiba	Main tremor	Largest aftershock	Aftershock in Fukushima	Aftershock in Ibaraki	Fukushima-hama
29	0.017	0.016	0.022	0.006	0.018	0.023	0.025
22	0.015	0.022	0.024	0.011	0.015	0.027	0.024
16					0.016		
8	0.016			0.006	0.016	0.023	0.021
Average	0.016	0.019	0.023	0.008	0.016	0.024	0.023
Overall average	0.018						

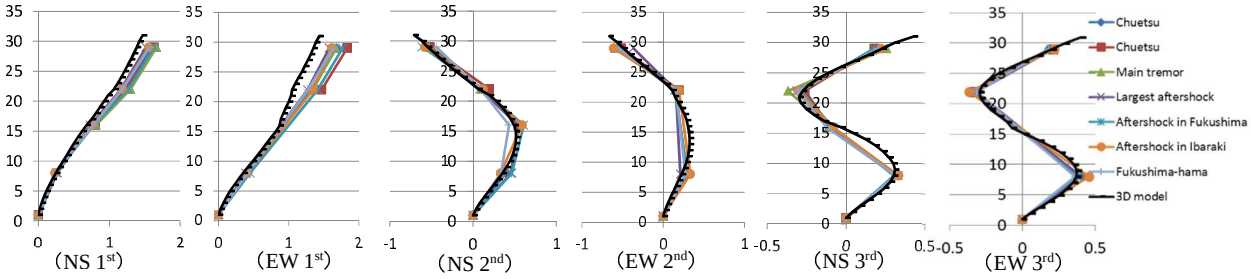

Fig. 6 Participation functions

Table 5 shows comparison of results of identification of the March 11 earthquake with the identification results of vibration characteristics of the building under research by Kasai and others. Slight differences are observed in damping coefficients of the second mode in the NS direction and the first mode in the EW direction, and the damping coefficients identified in this research are lower, but the results of this research coincide well with the ones by Kasai and others in other parts. The distinctive trend is that the damping coefficients of the second mode in the NS direction are low. Fig. 7 shows comparison between analysis of mode polymerization and observation records of acceleration with the use of identification values up to third modes on the 29th floor. From the well-matching around the peaks of the amplitude, it is assumed that the steel skeleton frame behaved around the elastic area. The changes in vibration characteristics, however, can be observed, since analytical values are larger before the peaks, and then the observation values are larger after the peaks both in the NS and EW directions.

Table 5 Comparison of natural periods and damping coefficients between this research and the one by Kasai and others in the Ref.3

		Natural periods(s*)		Damping coefficients						Participation functions					
		Average		29F		22F		16F		29F		22F		16F	
Direction	Mode	This research	Reference 3)	This research	Reference 3)	This research	Reference 3)	This research	Reference 3)	This research	Reference 3)	This research	Reference 3)	This research	Reference 3)
NS	1	3.09	3.10	0.018	0.020	–	–	0.019	0.021	1.667	1.770	–	–	0.811	0.867
	2	0.95	0.94	0.012	0.016	–	–	0.012	0.016	−0.522	−0.549	–	–	0.544	0.542
	3	0.47	0.47	0.032	0.034	–	–	0.035	0.034	0.260	0.252	–	–	−0.11	−0.053
EW	1	2.96	2.97	0.012	0.017	0.013	0.017	–	–	1.670	1.724	1.167	1.348	–	–
	2	0.99	1.00	0.022	0.021	0.024	0.021	–	–	−0.597	−0.572	0.108	0.123	–	–
	3	0.52	0.52	0.032	0.033	0.027	0.033	–	–	0.200	0.203	−0.370	−0.387	–	–

*Natural frequency in the Reference 3 is converted to the periods.

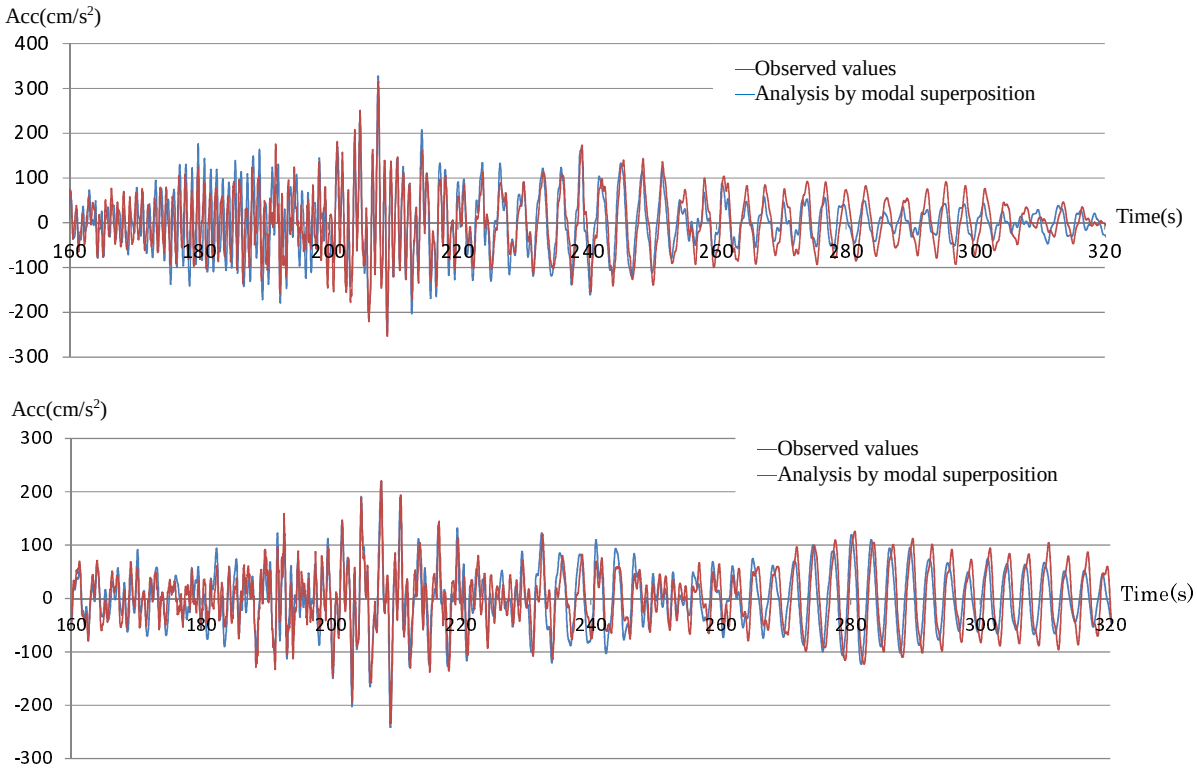

Fig. 7 Comparison of analysis by modal superposition and observation

4.2 Analysis of vibration characteristics

Table 4a shows obvious change in natural periods before and after the main shock and extension of the period after the main shock. The extension of the periods is estimated to have been mainly caused by the peeling of the fixation portion in non-structural elements such as exterior materials, partition walls and other parts. Below are reasons for this.

1) From the fact that there is slight difference between analysis by modal superposition of the main shock calculated from linear equation of motion and observation waveforms of acceleration (Fig. 7), it is estimated that the structure almost maintained the elasticity (similar description is also found in Ref. 3).
2) The unloading rigidity after plasticization of steel restored the elastic gradient, so the elastic rigidity did not deteriorate unlike a reinforced-concrete structure. Thus, if plasticization of steel causes the extension of periods, the natural periods in the event of an aftershock with a small amplitude after the main shock should restore the natural periods before the main shock. Additionally, plasticization causes hysteresis damping, but the damping in the first and second modes in the main shock did not particularly increase.

As the reason for the slightly longer natural period in the largest aftershock than the one in the main shock, it is assumed that the amplitude of the largest aftershock occurred after the natural period became longer and the amplitude was relatively large while the time history waveform used in the analysis of the main shock included the amplitude before the natural period became long immediately after the main shock occurred.

In comparison of the natural period at the time of the Niigata Prefecture Chuetsu Earthquake with the longest natural period at the time of the largest aftershock, it was 1.07 times in the first mode, 1.06 times in the second mode, and 1.07 times in the third mode in the NS direction, and 1.06 times in the first mode, 1.08 times in the second mode, and 1.05 times in the third mode in the EW direction. It is estimated that the rigidity deteriorated by approximately 10 to 15% in the event of the largest aftershock in comparison with the Niigata Prefecture Chuetsu Earthquake.

Fig. 8 shows damping coefficients and natural frequency of each earthquake in each mode (since if the horizontal axis is set as a natural period, it would be hard to grasp trends due to a bias of an interval of each mode, the natural frequency is used for the horizontal axis). The damping coefficients of the second mode in the main tremor and the earthquake which occurred in the Hama-dori, Fukushima Prefecture on April 11 significantly take a form of a valley in the NS direction, but it shows a reverse trend in the EW direction. Although the damping coefficient of the second mode in the EW direction of the largest aftershock is extremely low, the damping coefficient resulted in being identified low because the resonant peak of the second mode was steep and high as shown in the figure of Appendix 2. Overall, no noticeable characteristics in common are found with regards to changes before and after the main tremor.

The previous research reported that amplitude dependency was observed in the natural periods and damping coefficients[4, 5]. Amplitude of a mode in each earthquake is calculated with the use of the identified natural periods and damping coefficients. Eq. (2) shows a mode of the j mode after the mode development of the equation of motion with the multi-degree freedom system.

$$\ddot{q}_{oj} + 2h_j\omega_j\dot{q}_{oj} + \omega_j{}^2 q_{oj} = -\ddot{u}_o\,, \qquad q_{oj} = q_j \Big/ \beta_j \tag{2}$$

q_j indicates displacement amplitude of j th mode, and h_j and ω_j indicate values identified from the circular frequency corresponding to the damping coefficient and natural period. The data of acceleration measured on the first floor is used for $\ddot{u}_o$, the ground motion input. With the assumption of low amplitude dependency of β_j of the stimulus coefficient, although relatively compared, the size of the amplitude of the mode can be evaluated in comparison with the maximum value of q_{oj} of the mode of the same mode. The velocity amplitude (the velocity response spectrum) is used for organizing data below.

Fig. 9 shows the relation between the natural periods and the velocity amplitude of the mode in the first, second and third modes. They are positively correlated all in the first, second and third modes, and the extension of the natural period along with the increase in the amplitude is observed.

Fig. 10 indicates the relation between the damping coefficients and the velocity amplitude of the mode. The damping coefficient in the first and second modes is approximately around 0.01 to 0.02 in the NS direction regardless of the amplitude. The one in the third mode is positively correlated with the amplitude with the range of 0.017 to 0.032. The damping coefficient in the first and second modes varies considerably in the EW direction, and does not show clear correlation, but the one in the third mode is positively correlated with the amplitude in the same way as in the NS direction. Since the average of the two accelerographs is used for the data in the NS direction, the noise has relatively small influence on the result. The data in the NS direction thus varies slightly compared with the one in the EW direction.

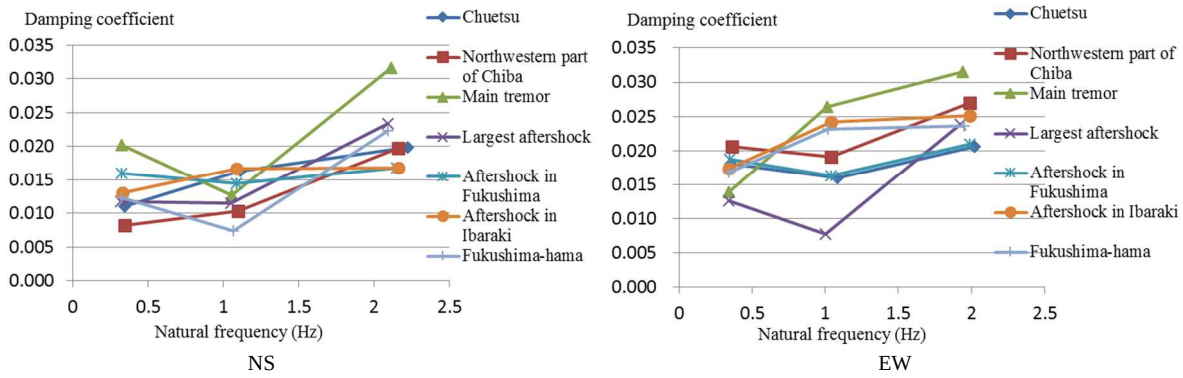

Fig. 8 Damping coefficient and natural frequency

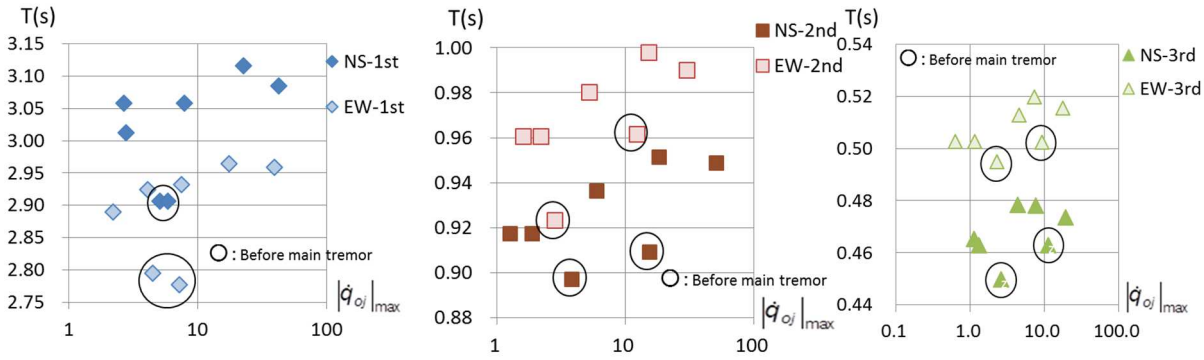

Fig. 9 Amplitude dependency of the natural period

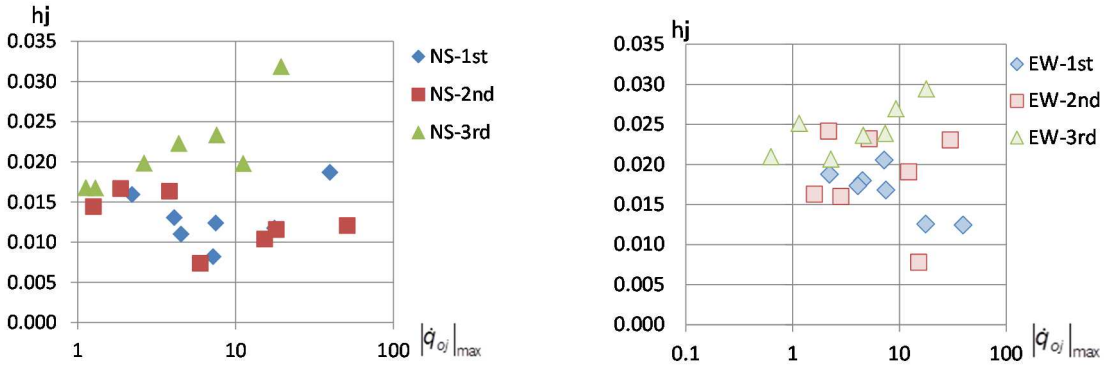

Fig. 10 Amplitude dependency of the damping coefficients

With the analysis about the overall trend by the average in all the earthquakes shown in Table 4b, the damping coefficients all in the first, second and third modes in the EW direction are slightly larger than the ones in the NS direction. The EW direction is the longitudinal direction which includes the super-truss, and is less deformable than the NS direction. However, the assumption that friction arising from the exterior materials, partition walls and the building frame causes damping can explain for the larger damping in the EW direction which is likely to have contact between the frame and these non-structural elements.

The building under research does not utilize vibration control dampers, and most of the damping coefficients for the first and second modes identified with regards to the main shock and the largest aftershock, except for the second mode in the EW direction are well below 0.02 which is conventionally assumed as damping for dynamic analysis of steel buildings against strong ground motion. In earthquakes such as the ones of a Tokyo inland earthquake which is feared to occur, long-period ground motions caused by a Tokai/Tonankai Earthquake which generate large-scale response well beyond the one by the off the Pacific coast of Tohoku Earthquake, the input energy is likely to be mostly consumed by damage of the building frame. Reduction of damage by damping is currently under examination[11].

5. CONCLUSION

This report identified the vibration characteristics of the 29-storied steel-frame building which was constructed in 1989 in Shinjuku with the application of the curve-fitting method using the transfer function from the observation record of acceleration before and after the off the Pacific coast of Tohoku Earthquake which occurred on March 11, 2011. The knowledge below is found from the identified result.

1) The natural periods in the event of the main shock increased by five to eight percent before the main shock. With the assumption that the reduction of rigidity was caused by the peeling of the non-structural elements, it is estimated that the non-structural elements contributed to about 10 to 15% of the rigidity in the event of the main shock before the main shock occurred.

2) The result of analysis of mode polymerization well matched with the observation record. The framework is also presumed to have almost elastically behaved at the time of the main shock.
3) On the one hand, the natural periods show amplitude dependency all in the first, second and third modes. On the other hand, the damping coefficient clearly indicates amplitude dependency only in the third mode, but the ones in the first and second modes are not found to be correlated with amplitude.
4) In the main shock as well, the damping coefficients for the 1st and 2nd modes are found to be smaller than 0.02 which is a conventional assumption in design of steel buildings except for the one for the second mode in the EW direction.

ACKNOWLEDGMENT

This research was conducted as part of research by the Research Center for Urban Disaster Mitigation (the "UDM"), Kogakuin University, and received its funding support.

APPENDIX 1 WAVEFORM OF ACCELERATION IN THE EVENT OF THE OFF THE PACIFIC COAST OF TOHOKU EARTHQUAKE

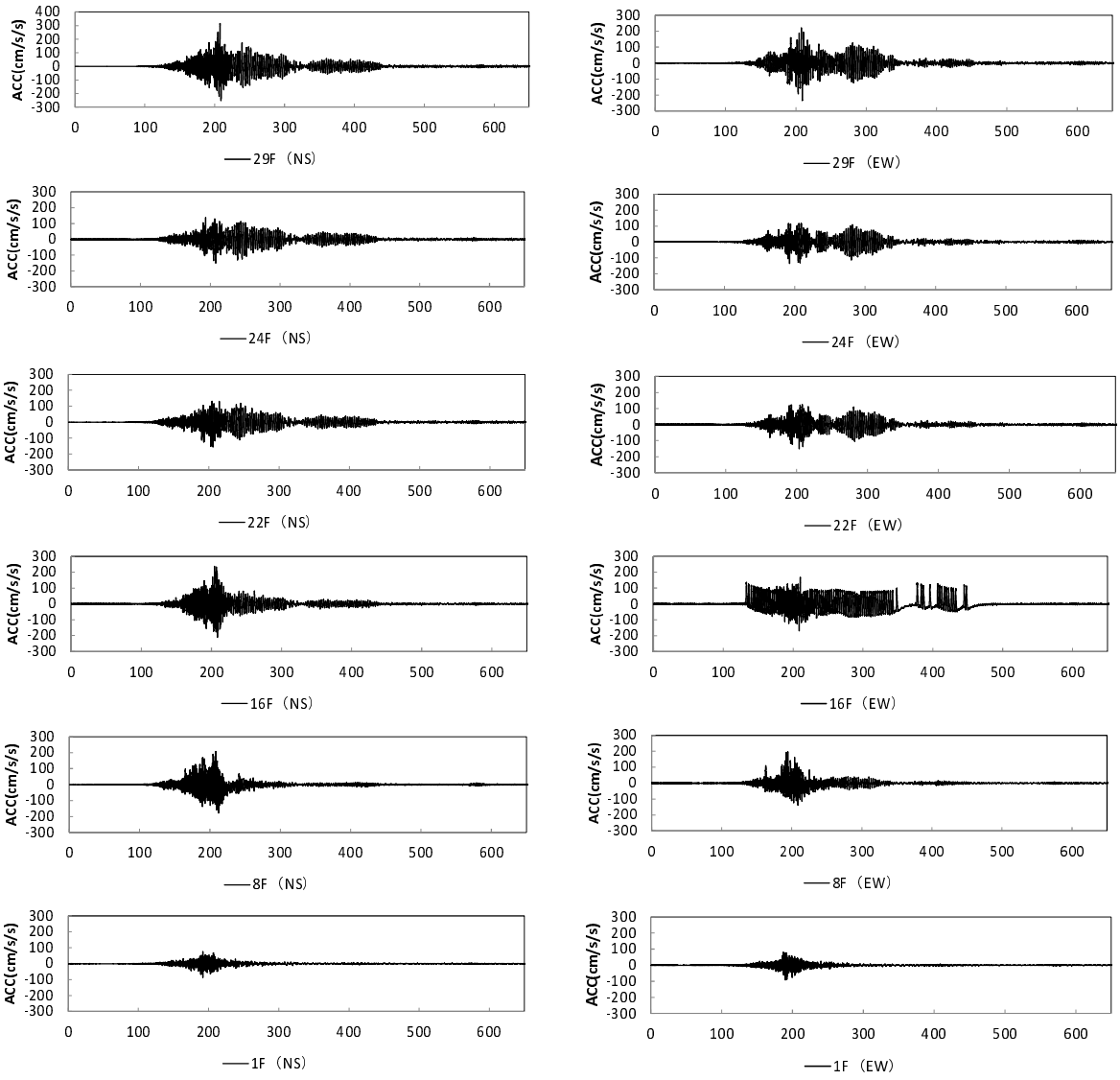

APPENDIX 2 RELEVANCE OF TRANSFER FUNCTIONS

(The main tremor shown here is the one in the NS direction on the 29th, 22nd, and 16th floors. The horizontal axis indicates frequency.)

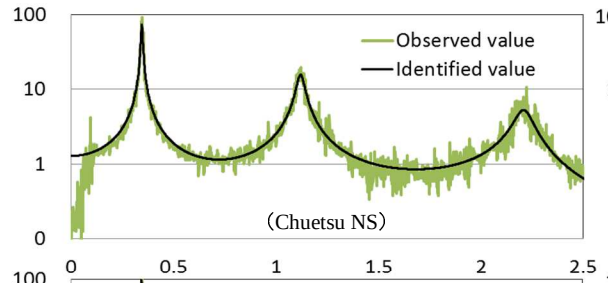

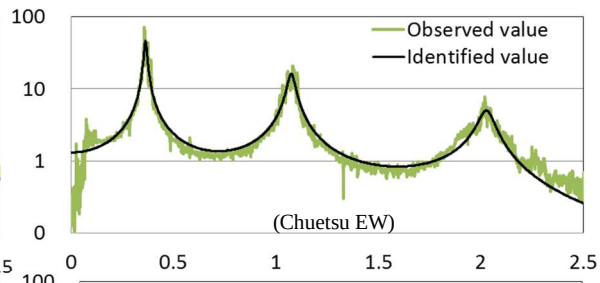

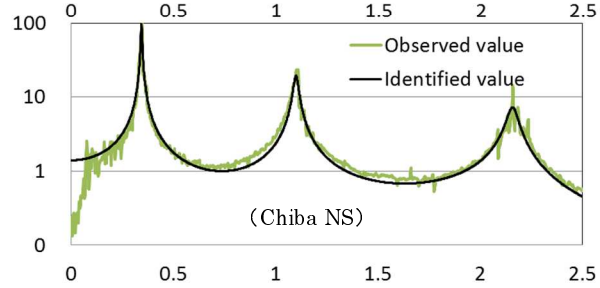

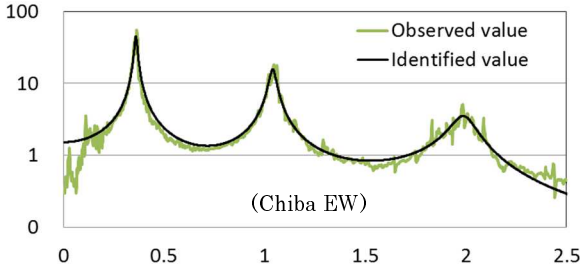

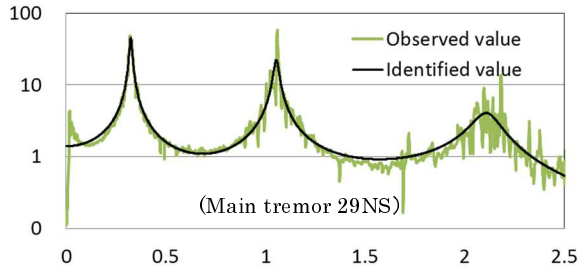

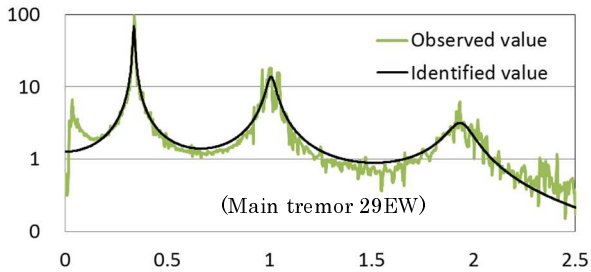

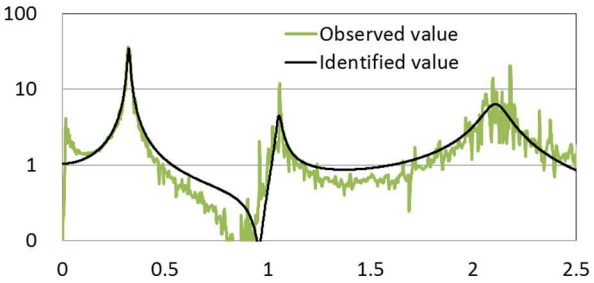

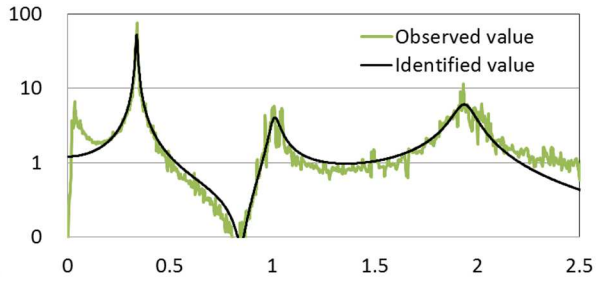

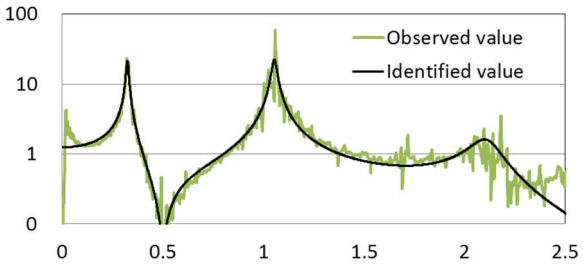

Not utilized due to the noise

(Main tremor 16EW)

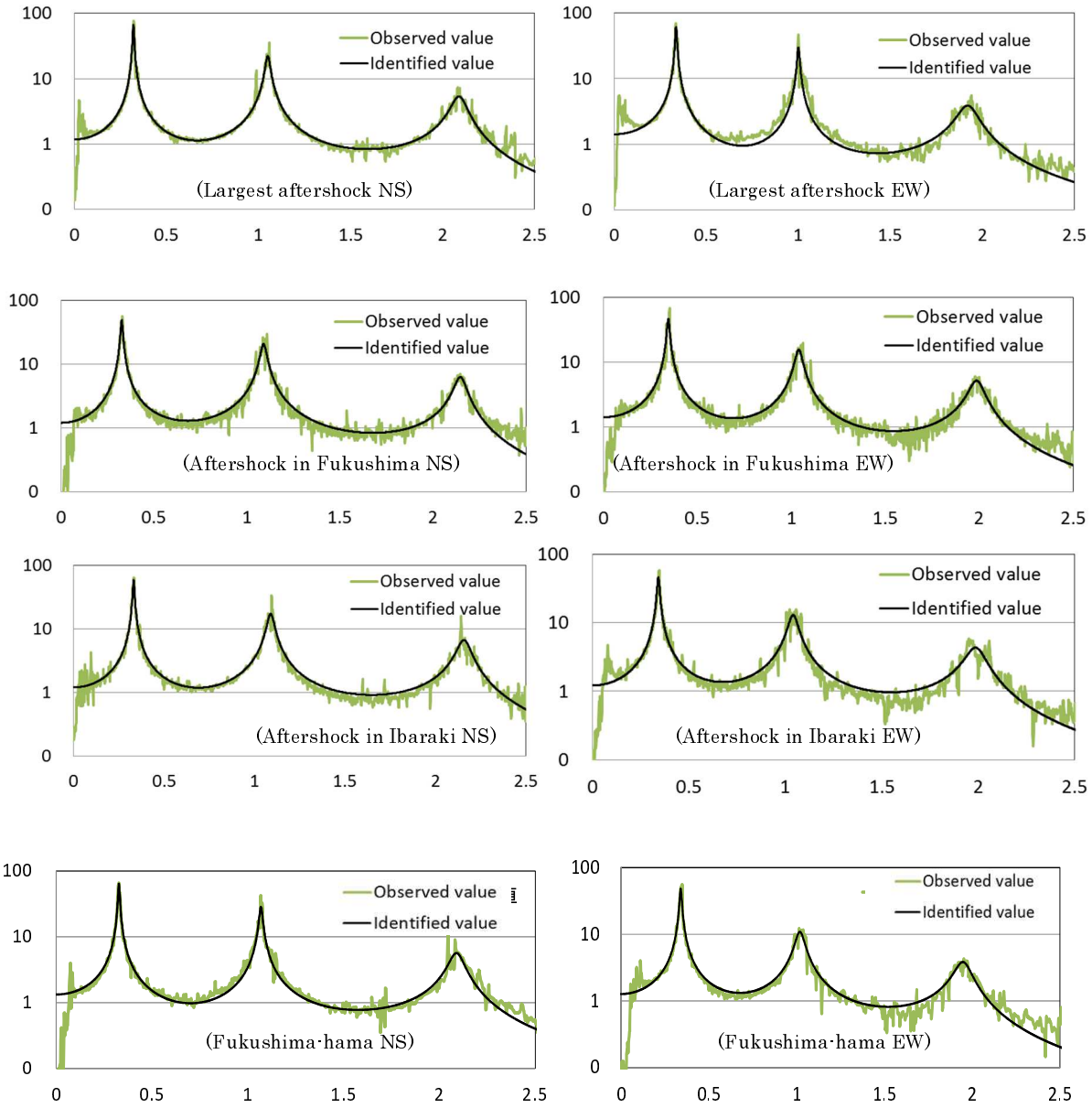

APPENDIX 3 3D ANALYSIS MODEL

The eigenvalue analysis is conducted with the use of the 3D analytical model (Figure 1a). SNAPVer.4[12] is used as the analysis software. This is limited to the aboveground model, and the details are referred to Reference [9]. Improvement to Reference [9] below is made for an increase in the precision

1) On the basis of the finite-element analysis of the plane of the brace structure, the elastic rigidity of the brace is 1.2 times as large as the rigidity whose length of flexibility is set as the length of the intersection of the material cores which does not include the size of a column-beam joint part and a gusset plate, but the one for the 14th and 21st floors, high floors, in the NS direction, is 1.0 time as large as such rigidity. This is due to deformation of the gusset plate itself and to the gusset plate's sinking into the BOX column[13].
2) The shearing deformation of the column-beam joint section is taken into account. Some reports say that shearing deformation of a column-beam joint section is relatively small in a node where a brace is installed because of the gusset plate[14], but all the nodes are considered in this report. The panel here, however, is an elastic one.

REFERENCES

1） Yoshiaki Hisada, Tetsuo Yamashita, Masahiro Murakami, Tomohiro Kubo, Jun Shindo, Koji Aizawa and Tatsuhiro Arata：Seismic response and damage of high-rise buildings in Tokyo、Japan, during the 2011 Great East Japan earthquake, JOINT CONFERENCE PROCEEDINGS, 9th International Conference on Urban Earthquake Engineering/ 4th Asia Conference on Earthquake Engineering、March, 2011, pp.227 (Full-text in CD)

2） Yoshiaki, Hisada.: The long-period earthquake which stroke Tokyo - a report from the area of super high-rise buildings at the western Shinjuku, The Immediate report of the Great East Japan Earthquake. Journal of architecture and building science, Vol.126, No.1618, May 2011, pp.5-8.

3） The Japan Society of Seismic Isolation: The report on research of buildings of response-control in the Tohoku-Pacific Ocean Earthquake, and research of buildings of response control, January 2012. (CD)

4) Haruhiko Yokota, Naoki Satake, and Kei-ichi Okada. Damping Properties of High-Rise Steel Buildings Based on Data of Vibration Tests And Earthquake Observation. Journal of structural and construction engineering, No. 453, November 1993, pp.77-84.

5） Toshihide Kashima, and Yoshikazu Kitagawa. Dynamic Characteristics of Buildings Estimated from Strong Motion Records. Journal of Architecture and Building Science, vol.22, December 2005, pp.163-166.

6） Yasunori Yamasaki, Nobuo Fukuwa, and Jun Tobita. A Study on Designed and Observed Values of Natural Periods and Damping Ratios of Tall Buildings. Summaries of technical papers of Annual Meeting Architectural Institute of Japan (Tokai), Structures II, September 2003, pp.947-948.

7） Yuichi Hirata, Yoshio Inoue, Toru Nagaoka, Masaharu Tanigaki, and Kuniaki Yamagishi. Earthquake Observation Results of High-Rise 50-storey Building Recorded in The Central Chiba Prefecture Earthquake of July 23, 2005. Summaries of technical papers of Annual Meeting Architectural Institute of Japan (Kanto) Structures II. September 2006. pp.149-150.

8）Satoshi Yamada, Yuta Ohkawara, Hiroaki Yamanaka, Hiroyasu Sakata, Hitoshi Morikawa, Yoji Ooki, Kazuhiko Kasai, and Akira Wada. Brief report on recorded seismic responses of a base-isolated tall building. Summaries of technical papers of Annual Meeting Architectural Institute of Japan (Kyushu) Structures II. August 2007. pp.963-964.

9) Yukio Hoshi, Yoshiaki Hisada, Tetsuo Yamashita, Yoe Masuzawa and Kenta Shimamura. Study on Vibration Characteristics of a High-rise Building using results of Microtremor, Manpower Excitation Measurements, Earthquake Observations and Simulations of a 3D Moment-frame structure. Journal of Japan Association for Earthquake Engineering, Vol. 10, No.2. May 2005. pp.73-88.

10) Kazuhiko Kasai, Shinichiro Murata, Fumito Kato, Tsuyoshi Hikino, and Yoji Ooki. Evaluation Rule For Vibration Period, Damping, and Mode Vector of Buildings Tested by a Shake Table With Inevitable Rocking Motions. Journal of Structural and Construction Engineering, Vol. 76, No. 670. December 2011. pp.2031-2040.

11) Tetsuo Yamashita, Yukio Hoshi, Yoshiaki Hisada, Yoe Masuzawa and Kenta Shimamura. Study on Vibration Characteristics of a High-rise Building using results of Microtremor, Manpower Excitation Measurements, Earthquake Observations and Simulations of a 3D Moment-frame structure. Journal of Japan Association for Earthquake Engineering. November 2010. pp.4006-4013.

12) KOZO System, Inc.: SNAP Ver.4 Technical Manual.

13)Yasumasa Ohko, Katsuhiro Nagafusa, Testuo Yamashita, and Yoshiaki Hisada. Strong Ground Motion Observation And Seismic Response Analysis On Super High-Rise Buildings In The 2011 Tohoku Region Pacific Ocean Coast Earthquake: Part 2: Structural modeling. Journal of Structural and Construction Engineering (Kanto) Structure II. September 2011. pp.307-308.

14) Shoichi Kishiki, Yasushi Ichikawa, Satoshi Yamada, and Akira Wada. Experimental Evaluation of Structural Behavior of Gusset-Plate Connection: Grobal enhancement of seismic performances of passive-controlled structures Part 1. Journal of Structural and Construction Engineering vol.620. October 2007. pp.133-140.

15) Tomohiro Kubo, and Yoshiaki Hisada. Study on Earthquake Disaster Mitigation of High-Rise Building of University Campus in Tokyo, Japan, by collaborating with local communities (Part 6): Quickly estimation method of Long-period Ground Motion for the Elevator Emergency Operation Control using the Early Earthquake Warning System. Journal of Structural and Construction Engineering (Tohoku) Structure II. September 2008. pp.823-824.

(Original Japanese Paper Published: September, 2012)
(English Version Submitted: September 30, 2014)
(English Version Accepted: November 10, 2014)